Published in final edited form as:
NMR Biomed. 2014 March ; 27(3): 253–260. doi:10.1002/nbm.3058.

Quantitative magnetization transfer imaging of rodent glioma using selective inversion recovery

Junzhong Xu[a,b,*], **Ke Li**[a,b], **Zhongliang Zu**[a,b], **Li Xia**[a,b], **Daniel F. Gochberg**[a,b,c], and **John C. Gore**[a,b,c,d,e]

[a]Institute of Imaging Science, Vanderbilt University, Nashville, TN 37232, USA

[b]Department of Radiology and Radiological Sciences, Vanderbilt University, Nashville, TN 37232, USA

[c]Department of Physics and Astronomy, Vanderbilt University, Nashville, TN 37232, USA

[d]Department of Biomedical Engineering, Vanderbilt University, Nashville, TN 37232, USA

[e]Department of Molecular Physiology and Biophysics, Vanderbilt University, Nashville, TN 37232, USA

Abstract

Magnetization transfer provides an indirect means to detect variations in macromolecular contents in biological tissues non-invasively, but so far, there have been only a few quantitative MT (qMT) studies reported in cancer, all of which used off-resonance pulsed saturation methods. This paper describes the first implementation of a different qMT approach, selective inversion recovery (SIR), for characterizing tumor *in vivo* using a rodent glioma model. The SIR method is an on-resonance method capable of fitting qMT parameters and T_1 relaxation time simultaneously without mapping B_0 and B_1, which is very suitable for high field qMT measurements due to lower saturation absorption rate. The results show that the average pool size ratio (PSR, the macromolecular pool vs. the free water pool) in rat 9L glioma (5.7%) is significantly lower compared with normal rat gray matter (9.2%) and white matter (17.4%), which suggests PSR is potentially a sensitive imaging biomarker for assessing brain tumor. Despite being less robust, the estimated MT exchange rates also show clear differences from normal tissues (19.7 Hz for tumors vs 14.8 and 10.2 Hz for grey and white mater respectively). In addition, the influence of confounding effects, e.g. B_1 inhomogeneity, on qMT parameter estimates is investigated with numerical simulations. These findings not only assist better understanding of the changes in the macromolecular contents of tumors, but also are important for interpreting other imaging contrasts such as chemical exchange saturation transfer (CEST) of tumors.

Keywords

quantitative magnetization transfer; selective inversion recovery; pool size ratio; exchange rate; chemical exchange; cancer; 9L

INTRODUCTION

Magnetization transfer (MT) in general describes spin exchange processes between nuclei in different environments, but MT imaging is usually interpreted as exchange between

[*]Corresponding author: Address: Vanderbilt University, Institute of Imaging Science, 1161 21st Avenue South, AA 1105 MCN, Nashville, TN 37232-2310, United States. Fax: +1 615 322 0734. junzhong.xu@vanderbilt.edu (Junzhong Xu).

macromolecular and free water proton pools via dipolar interactions and/or chemical exchange. The magnetization transfer ratio (MTR) (1) was defined as a semi-quantitative metric of the contrast available from simple MT weighting of MRI signals. The macromolecular proton signal is largely invisible in conventional MRI acquisitions, so the MTR provides an indirect measurement of macromolecular contents in biological tissues. The macromolecular content of tissues varies during the progression of several diseases, so MTR imaging has been successfully applied to, for example, neurological disorders (2), liver fibrosis (3), neuromuscular diseases (4), and cancer (5–9).

Although MTR has been found to be useful in practice and to correlate with various pathological changes, MTR values are also sensitive to various experimental parameters, including the RF irradiation power, frequency offset, and tissue relaxation properties, which reduce the specificity to changes in macromolecular contents. More importantly, these confounding parameters are user specific and the inability to standardize methods hinders general clinical applications, especially in large scale multiple-site clinical trials. Furthermore, even if MTR acquisition parameters universally adhered to a standard as suggested previously (10,11), the MTR metric is inherently sensitive to multiple tissue properties and hence fails to distinguish between, for example, changes in the PSR (pool size ratio, i.e. the ratio of protons in the macromolecular pool to those in the free water pool) and R_1. In order to reduce this dependence on acquisition parameters, and to increase the biophysical specificity, quantitative magnetization transfer (qMT) imaging has been developed to quantify intrinsic MT parameters, including relaxation rates, PSR, and MT exchange rates (12–14). Several different approaches of qMT imaging have been reported, including conventional continuous-wave (12) and pulsed saturation (14) methods using RF pulses with multiple frequency offsets and/or amplitudes. Distinct from these steady-state approaches, the selective inversion recovery (SIR) (13,15) is a transient, on-resonance qMT technique, in which an on-resonance RF pulse is applied to selectively invert the free water protons. The resulting transient longitudinal magnetization can be measured and fit to a bi-exponential recovery (16) from which the intrinsic MT parameters can be estimated. Unlike conventional continuous-wave and pulsed saturation qMT methods, the SIR qMT approach does not require extra mapping of B_0, B_1, and conveniently, T_1 and qMT parameters can be fit simultaneously. The SIR technique has previously been applied to quantify MT parameters in phantoms (17), ferret (18), rat (19) and human brain (20,21), and human skeletal muscles (22) in vivo.

In the last two decades, MTR has been widely adopted in cancer imaging, including imaging studies of cerebral (5,8), prostate (9), pancreatic (6), and breast cancers (7). However, only a small number of studies of cancer using qMT have been reported (8,23–25) and these all used the pulsed saturation qMT method. No systematic studies of tumors have been previously reported using the SIR approach. In addition to assessing changes in macromolecular content in tumors, quantitative mapping of MT parameters may also be important for better understanding changes relevant for other imaging methods. For example, the quantification of chemical exchange saturation transfer (CEST) imaging data suffers significantly from MT asymmetry effects on the measured signals (26), while the interpretation of CEST measurements of protein amides may be affected by whether concomitant variations occur in total protein content. In the current study, qMT measurements using the SIR approach have been applied to assess tumor characteristics for the first time using a rodent glioma model. A new SIR-EPI sequence was developed to ensure a minimal repetition time can be achieved to significantly accelerate the image acquisition. The fitted qMT parameters are consistent with previously published results. Both the PSR and MT exchange rates are potentially sensitive imaging biomarkers for detecting tumors and assessing the state of tissues. In addition, maps of T_2 and ADC

(apparent diffusion coefficient) were also acquired and correlated with the qMT data, which may be helpful for better understanding of MT contrast in tumors.

THEORY

Selective Inversion Recovery (SIR) qMT

Biological tissues are considered to be comprised of two pools of protons, a free water pool (f) and a macromolecular pool (m), and each pool has unique equilibrium magnetizations ($M_{f\infty}$ and $M_{m\infty}$) and spin-lattice relaxation rates (R_{1f} and R_{1m}). MT can occur between the pools and may be modeled by adding coupling terms to the Bloch equations (17). The recovery of the free pool longitudinal magnetization $M_f(t)$ can then be described by a bi-exponential function

$$\frac{M_f(t)}{M_{f\infty}} = b_f^+ e^{-R_1^+ t} + b_f^- e^{-R_1^- t} + 1 \quad [1]$$

where R_1^+ and R_1^- are the fast and slow recovery rates, respectively, of the overall recovery. Note that R_1^- is the conventional spin-lattice relaxation rate when measured with an inversion recovery experiment, since most studies use inversion times $\gg 1/R_1^+$. If k_{fm} is the MT exchange rate from the free to the macromolecular pool and k_{mf} is the rate in the reverse direction, all parameters in Eq.[1] can be solved analytically, i.e.

$$2R_1^{\pm} = R_{1f} + R_{1m} + k_{fm} + k_{mf} \pm \sqrt{(R_{1f} - R_{1m} + k_{fm} - k_{mf})^2 + 4k_{fm}k_{mf}} \quad [2]$$

and

$$b_f^{\pm} = \pm \frac{\left[\frac{S_f M_f(0^-)}{M_{f\infty}} - 1\right]\left(R_{1f} - R_1^{\mp}\right) + \left[\frac{S_f M_f(0^-)}{M_{f\infty}} - \frac{S_m M_m(0^-)}{M_{m\infty}}\right] k_{fm}}{R_1^+ - R_1^-}, \quad [3]$$

where subscripts f and m represent free and macromolecular pools, respectively. R_{1f} and R_{1m} are spin-lattice relaxation rates, and $M_f(0^-)$ and $M_m(0^-)$ are magnetizations before the inversion pulse, which have experienced a longitudinal recovery with a pre-delay time t_d. Note that the inversion pulse may not completely invert the longitudinal magnetization of the free pool, and may also have some influence on the macromolecular pool, so two more parameters (the inversion coefficients S_f and S_m,) must be introduced to account for these effect. Using Eq.[1–3], the qMT parameters, e.g. pool size ratio (PSR = $M_{m\infty}/M_{f\infty}$.) and exchange rate k_{mf} ($k_{fm} = k_{mf} \times$ PSR) can be quantified by fitting the measured signals to a bi-exponential recovery.

SIR-EPI with saturation pulse train

SIR-qMT acquisitions were first evaluated using phantoms consisting of cross-linked bovine serum albumin (BSA) using echo planar imaging (EPI) with long repetition times chosen so that long pre-delay times $t_d \approx 5 * T_1$ ensured a full recovery of $M_f(t)$ between scans (17). However, such long repetition times significantly increase the total scan time, which would make this approach not clinically feasible. A fast spin echo (FSE) acquisition has been proposed (18), in which the longitudinal magnetizations of both the free and macromolecular pools are saturated and are approximately zero at the end of the FSE readout, so that a much shorter pre-delay time as well as a much shorter repetition time can

be used. The effect of the partial recovery of $M_f(t)$ in the shorter pre-delay period can be accounted in the signal model so that all SIR-qMT parameters may still be quantified without bias (18). This technique significantly reduces the pre-delay time t_d and the total scan time, and has previously been successfully applied in imaging of rat (18,19) and human brain (20) in vivo.

In the current study, a new SIR-EPI sequence was introduced to combine the advantages of the fast acquisition of EPI and short pre-delay time of SIR-FSE. Specifically, the EPI readout scheme that acquires qMT data was followed by a saturation pulse train consisting of multiple 180 ° pulses (see Figure 1). The EPI readout ensures fast acquisitions, while the train of saturation pulses ensures a short repetition time can be used. Such a sequence can further accelerate the acquisition of SIR-qMT experiments compared to SIR-FSE methods but preserve the ability to estimate qMT parameters without bias. Note that the repetition time in this sequence is dynamic and minimized in each scan to different values depending on t_i and t_d. Hence, it avoids the conventional long waiting periods when short t_i and/or t_d are used, and significantly increases acquisition efficiency. A similar technique of using a saturation pulse train in SIR sequences was reported recently for human brain imaging at 7T (21). However, that method used pulses of different flip angles (135°) and a turbo field echo readout which can slightly bias the estimation of qMT parameters (21).

MATERIALS AND METHODS

Animal preparation

9L glioblastoma cells were obtained from American Type Culture Collection (ATCC 9L/lacZ, CRL-2200) and grown in Dulbecco's modified Eagle's medium (DMEM; Gibco, Gaithersburg, MD) with 10% fetal calf serum and 500 μg/ml penicillin. Cells were maintained in a humidified incubator at 37 °C with 5% CO_2.

All animal related procedures were approved by our Institution's Animal Care and Use Committee. Eight male Fischer 344 rats (250 – 300 grams) were immobilized and anesthetized with a 2%/98% isoflurane/oxygen mixture. The rats were inoculated with 1×10^5 9L glioblastoma cells in 5 μl of DMEM using a 10 μL gastight syringe ~1 mm anterior and 2 mm lateral to the bregma on the right side of the head, at a depth of 4 mm relative to the dural surface. Rats were imaged 14 – 18 days after intracranial inoculation depending on the size of tumors developed. More details of these procedures have been reported previously (27).

In Vivo MRI experiments

Animals were anesthetized with isoflurane (3% for induction and 2% during the imaging experiments) and fixed in a MRI compatible cradle with bite and head bars. Rectal temperature was maintained at around 37 °C using a warm-air feedback system throughout the experiment. A birdcage RF coil with 38 mm internal diameter was used for both the transmitter and receiver.

All experiments were performed on a 9.4T Agilent MRI scanner (Agilent Technologies Inc., Santa Clara, CA) using a 2-shot spin-echo echo-planar imaging (EPI) sequence with the number of excitations equal to 2. A triple reference imaging scheme (28) was used to reduce EPI artifacts, with two phase-encoded images with reversed readout and phase-encoding directions and two corresponding non-phase-encoded phase maps. A single axial slice crossing the center of tumor was acquired with a slice thickness of 2 mm. Field-of-view = 32 × 32 mm, and matrix size 96 × 96, yielding an isotropic in-plane resolution of 333 μm. Both spin-lattice relaxation time T_1 and multiple qMT parameters were obtained using the SIR-

EPI sequence shown in Figure.1. Specifically, a 1 ms hard inversion pulse was applied to invert the longitudinal magnetization of the free water pool. There were 20 inversion times used in the current study which were logarithmically distributed over the range from 5 ms to 10 sec, while the pre-delay time t_d was kept constant at 3.5 sec. The saturation pulse train had 10 refocusing pulses with an echo spacing of 10 ms. Previous computer simulations verified that longitudinal magnetization will be completely saturated at the end of the echo train (18). The total scanning time for qMT measurements was less than 14 minutes.

In addition, maps of spin-spin relaxation times T_2 were obtained using spin-echo EPI with multiple echo times, i.e. 30, 40, 60, 80, and 100 ms. ADC (apparent diffusion coefficient) maps were obtained using a pulsed gradient spin echo sequence with a gradient duration (δ) 5 ms and separation (Δ) 12 ms, and fitted mono-exponentially with four b values (400, 600, 800, and 1000 s/mm^2).

Data analysis

All data analyses were performed with programs written in MATLAB (Mathworks, Natick, MA). For each animal, all images were co-registered to the corresponding SIR-EPI image acquired at t_i = 10 sec using a rigid body registration algorithm by maximizing the normalized mutual information (29). Following co-registration, the brain region was manually selected for further data fitting. All MR parameters, including SIR-qMT, T_2 and ADC, were fitted on a pixel-wise basis. The SIR-qMT signal model described in Eq. [1–3] has seven independent parameters: R_{1f}, R_{1m}, S_f, S_m, $M_{f\infty}$, PSR, and k_{mf}. As shown in previous studies (19), R_{1m} can be set equal to R_{1f} due to the week dependence of SIR signals on R_{1m}. To further enhance fitting simplicity, numerical simulations were performed to provide S_m as 0.83 for the 1 ms hard inversion pulse used in the current study (18). Therefore, five parameters, i.e. R_{1f}, S_f, $M_{f\infty}$, PSR, and k_{mf}, were fitted from SIR-EPI data using a least-squares method. The spin-lattice relaxation time T_1 was calculated simultaneously. ROIs (regions of interest) of tumor, GM (grey matter) and WM (white matter) were manually selected from the T_1 map of each rat, and ROI-based group analyses were also performed to investigate the feasibility of using qMT parameters to differentiate different types of tissues.

Computer Simulations

To investigate the influence of the saturation echo train, B_1 inhomogeneity and relaxation times on the fitted qMT parameters, computer simulations were performed based on solving six coupled differential equations (30). The simulations mimicked the actual imaging experiments so that all pulse sequence parameters including the 20 inversion times were the same as those used in the actual MRI scanning. The intrinsic qMT and relaxation parameters were set to the experimental fitted values (shown in Table 1) except that R_{2m} was 100kHz (18).

RESULTS

Figure 2a shows eight SIR-EPI images of a representative rat from a total of 16 images with different inversion times. The SIR signals of four typical ROIs, i.e. GM, WM, tumor and contralateral normal brain tissue, and the corresponding fitted curves obtained using Eq.[1–3] are shown in Figure 2b. All signals were normalized by the corresponding signals at the longest inversion time 10 sec. For visualization purposes, a magnified image only with short (< 250 ms) inversion times is inserted in Figure 2b which shows excellent agreement between the SIR-qMT data (open markers) and the bi-exponential recovery model of Eq.[1–3] (solid lines). It is clear that the tumor shows a very different bi-exponential recovery behavior in addition to its different recovery rate R_1.

Figure 3 shows representative parametric maps overlaid on a corresponding spin-echo EPI image. All parameters, T_1, T_2, ADC, PSR, k_{mf} and k_{fm} provide clear imaging contrast to differentiate tumor, GM and WM tissues, although the overall k_{mf} and k_{fm} maps are much more noisy as found previously (20). For a clear comparison, Table 1 summarizes all ROI-based parameter means and their standard deviations for all animals. As expected from multiple earlier studies, T_1 was significantly increased in tumor. However, by contrast, T_2 was found to be lower in the 9L tumor region at this field, which is opposite to previous observations at 4.7T (31). The ADC was higher in the tumor region, suggesting a lower cellularity compared to normal tissues. The PSR was significantly lower in the tumor, which is consistent with a few previously reported observations that used different qMT acquisition methods (8,23–25). The k_{mf} and k_{fm} maps show clear contrast between grey and white matters and higher values within the tumor, but the overall signal-to-noise ratios are much lower.

Figure 4 shows pixel-wise correlations between SIR-qMT parameters (PSR, k_{mf} and k_{fm}) and conventional MRI parameters ($R_1=1/T_1$, $R_2=1/T_2$, and ADC) from a representative rat. It is clear that PSR shows strong correlations with conventional MRI parameters, i.e. R_1 and R_2 with $p<0.01$ of Pearson's correlation. Interestingly, although the MT exchange rates, k_{mf} and k_{fm}, show significant correlations with R_1 and ADC, there is no significant correlation between k_{mf} / k_{fm} and R_2 ($p=0.08$ and $p=0.27$, respectively). Note that increasing PSR correlates positively with R_1 but negatively with R_2, suggesting that the factors dominating R_2 differ from those affecting R_1. The similar analysis was performed on all other rats and similar results were observed (data not shown).

Figure 5 summarizes the results of measured PSR and MT exchange rates in ROIs in all eight rats. Balanced one-way ANOVA analyses suggested the mean differences of qMT parameters, i.e. PSR, k_{mf} and k_{fm}, of different type of tissues were highly significant ($p < 10^{-12}$, $<10^{-7}$, and $<10^{-6}$, respectively). In addition, a multiple comparison procedure with the Bonferroni correction was performed to evaluate the difference between each pair of tissues, and the corrected p values are tabulated in Table 2. All Bonferroni-corrected p values are much smaller than 0.05, suggesting all three qMT parameters provide highly reliable ways to differentiate tissue types from each other. For comparison, previously reported PSR and k_{mf} of a healthy rat using the SIR-qMT method were (19): PSR of 0.080 ± 0.008 in GM and 0.173 ± 0.023 in WM, while k_{mf} of 20.8 ± 6.5 Hz in GM and 13.1 ± 2.9 Hz in WM. Therefore, although k_{mf} values are slightly different in the current work, our fitted MR parameters were in good agreement with previous results. For qMT parameters in tumor, PSR was measured to be 0.040 ± 0.002 in C6 gliomas using the pulsed saturation qMT method (25), which is close to the PSR of 9L tumors obtained in the current study using the SIR-qMT method, and both are significantly lower compared with those of normal tissue.

Figure 6 shows the influence of saturation echo train, B_1 inhomogeneity and relaxation times on the fitted qMT parameters. At $\Delta B_1=0$ (i.e. perfect RF pulses), fitted PSR's of all three types of tissues have <3.5% relative differences from the intrinsic values, suggesting that the saturation echo train used in the current SIR-EPI sequence does not influence the estimates much. Within ±20% errors of B_1 field, the relative errors of fitted PSR are within the range of +3.0% and −8.7% of intrinsic values. While k_{mf} seems insensitive to B_1 inhomogeneity (< 1.1% different from intrinsic value). k_{fm} was calculated from k_{mf} and PSR, so the relative percentage errors of k_{fm} are similar to those of fitted PSR values. Interestingly, the percentage errors of all fitted qMT parameters of three different types of tissues are similar to each other despite the significant difference in relaxation times. This suggests the parameter fitting depicted in Eq.[1–3] is robust in the face of variations of other confounding factors in practice.

DISCUSSION

This study demonstrates the feasibility of performing SIR-qMT measurements in tumors *in vivo*, and provides insights into the biophysical changes that characterize 9L tumors in rats. Although MTR has been widely used in cancer studies, only a few qMT imaging studies of tumors have been reported using the pulsed saturation method, while the SIR-qMT method has not been applied to tumors previously. Compared to the pulsed saturation qMT method, the SIR qMT method has a significant shortcoming in that multi-slice imaging is difficult (though 3D approaches are feasible) because the refocusing pulses in the saturation train can cause MT effects in neighboring slices (20). However, the SIR-qMT method has advantages when only a few slices are required for a limited coverage, e.g. tumors. Since T_1 and MT parameters can be obtained simultaneously, the SIR-qMT method might be a promising technique to perform qMT cancer imaging. In addition, pulsed saturation and SSFP-based qMT approaches may be difficult to implement on high field human scanners due to RF power limitations and magnetic field inhomogeneities, while the SIR-qMT technique can be implemented at ultra-high field strength for higher signal-to-noise ratio (20).

In the previous qMT imaging of tumors, Underhill et al. used a different rodent glioma C6 model but also found a significant decrease of PSR in tumors. Interestingly, they also found that tumors had lower ADCs in their study, suggesting a higher cellular density without increased macromolecular content compared to normal brain tissue, consistent with earlier studies of higher water content in tumor cells (32). However, ADC was found in the current study to be higher in the 9L tumor which has also been reported previously (27). Although several other factors may also affect the ADC of tissue, the above observations may indicate that a tumor may have a higher or lower cellularity depending on different tumor types and/or different stages. However, whatever the value of the ADC, all of the above studies showed that PSR in tumor is significantly lower compared to normal tissue. This agrees with previous studies suggesting that macromolecular content is more dilute in rapidly growing tissues and tumors, and is consistent with the conventional explanation for increased values of T_1 in tumors (33). The finding that T_2 is shorter in tumors is at first sight anomalous, and disagrees with a large body of earlier literature (34), but those studies were performed at substantially lower fields. Moreover, lower PSR would predict that T_2 would also be longer, just as found for T_1, as long as the same mechanisms of relaxation are dominant for both longitudinal and transverse relaxations. Clearly this cannot be the case, but the paradox is resolved if the dominant relaxation process for T_2 relaxation is chemical exchange rather than dipole-dipole interactions. We have previously shown that the relaxivity of diamagnetic proteins increases dramatically at high fields as chemical exchange contributions take over from other processes (35), and in the case of our 9L tumor it appears that the relaxation efficacy of the macromolecular content increases more than the amount of solid material decreases. One way in which this can occur is if the rate of exchange (or the chemical shift difference) between exchanging protons and water increases in tumors. Such an effect can arise if e.g. there are appropriate changes in pH or protein degradation. This conclusion is further validated by the apparent increase in the rate of magnetization transfer k_{mf}, which indicates that there is much faster transfer of magnetization from macromolecules to water in tumors compared to normal tissues.

These findings are relevant for the interpretation of other studies such as chemical exchange saturation transfer (CEST) imaging of tumors. CEST provides molecular imaging contrast and detects endogenous mobile molecules with high spatial resolution, and has shown potential for detecting cancer (34) and monitoring tumor response to treatment (36). Our results would suggest that an increase in CEST in tumors may not reflect an increase in macromolecular content but rather an increased rate of exchange and longer T_1 values, which has been found previously (37).

Although the precise mechanism of MT in tumors is not fully understood, both current and previous studies have suggested that PSR in tumors is significantly lower compared to normal brain tissues. QMT measurements may potentially provide more specific information on the content of the tumor microenvironment than relaxation times alone. Moreover, qMT may also potentially be useful for detecting changes in tumors following some treatments if they cause significant changes in macromolecular content, such as increases in the development of polyploidy (38) or decreases during apoptosis (39).

The saturation echo train in the current study significantly reduces the total acquisition time but only induces a small error to the fitted qMT parameters. More RF pulses in the saturation echo train can further reduce the induced errors, but this in turn will increase scanning time and, more importantly, increase SAR (specific absorption rate) which could be a problem for high field clinical studies. With ±20% errors of ideal B_1 field, the simulations show that the fitted PSR has <8.7% errors while k_{mf} has <1.1% errors. This suggests that the SIR-EPI method is a reliable means to measure qMT parameters in practice. The fact that the fitted qMT parameters are insensitive to relaxation times is encouraging, which shows that SIR-EPI can provide robust measurements of qMT parameters despite the significant relaxation variations in tumors or other lesions.

There were altogether 20 different inversion times (t_i) used in the current work and the pre-delay time t_d kept constant. Such a scheme provides an excellent fitting of bi-exponential recovery signals, but requires longer scanning time. It is possible to use the Cramer-Rao lower bound method to optimize both t_i and t_d in order to achieve minimized scanning time. We have previously shown that only 5 measurements are required to fit SIR qMT data in a healthy rat if T_1 is the range of 0.67 – 2 sec (19). Tumors have significantly different T_1 relaxation times and MT parameters, such as T_1 ~2.3 sec in this study. Hence, the previously optimized parameters may not be appropriate for imaging tumor-bearing rats. A new optimization which covers a larger range of T_1 and MT parameters is currently under development to speed up future SIR-qMT measurements in cancer imaging.

CONCLUSIONS

Quantitative magnetization transfer imaging using selective inversion recovery has been implemented in a rodent glioma model. All signals were well explained by the bi-exponential recovery model. The fitted quantitative MT parameters suggest that tumor has much lower macromolecular contents and higher MT exchange rate, which are consistent with previously reported results. This suggests that SIR-qMT can potentially serve as an imaging biomarker to detect changes in the microenvironment in tumor and hence potentially is able to monitor tumor response to treatment. These results also assist in clarification of the contrast reported in CEST imaging of tumors.

Acknowledgments

This study was supported by NIH K25CA168936, R01CA109106, R01CA173593, R01EB000214 and P50CA128323. The authors thank Ms. Zou Yue for assistance in animal surgeries.

Abbreviations

qMT	quantitative magnetization transfer
SIR	selective inversion recovery
PSR	pool size ratio

k_{mf}	exchange rate from macromolecular pool to free water pool
k_{fm}	exchange rate from free water pool to macromolecular pool
WM	white matter
GM	grey matter

References

1. Wolff SD, Balaban RS. Magnetization transfer contrast (MTC) and tissue water proton relaxation in vivo. Magn Reson Med. 1989; 10(1):135–144. [PubMed: 2547135]
2. Filippi M, Rocca MA. Magnetization Transfer Magnetic Resonance Imaging in the Assessment of Neurological Diseases. Journal of Neuroimaging. 2004; 14(4):303–313. [PubMed: 15358949]
3. Aisen AM, Doi K, Swanson SD. Detection of liver fibrosis with magnetic cross-relaxation. Magn Reson Med. 1994; 31(5):551–556. [PubMed: 8015410]
4. McDaniel JD, Ulmer JL, Prost RW, Franczak MB, Jaradeh S, Hamilton CA, Mark LP. Magnetization Transfer Imaging of Skeletal Muscle in Autosomal Recessive Limb Girdle Muscular Dystrophy. J Comput Assist Tomogr. 1999; 23(4):609–614. [PubMed: 10433295]
5. Niemi P, Kurki T, Lundbom N, Kormano M. Magnetization transfer contrast in Gd-DTPA-enhanced imaging of brain tumors. Investigative radiology. 1991; 26 (Suppl 1):S248–249. discussion S253–244. [PubMed: 1808140]
6. Li W, Zhang Z, Nicolai J, Yang GY, Omary RA, Larson AC. Magnetization transfer MRI in pancreatic cancer xenograft models. Magn Reson Med. 2012; 68(4):1291–1297. [PubMed: 22213176]
7. Abramson RG, Arlinghaus LR, Weis JA, Li X, Dula AN, Chekmenev EY, Smith SA, Miga MI, Abramson VG, Yankeelov TE. Current and emerging quantitative magnetic resonance imaging methods for assessing and predicting the response of breast cancer to neoadjuvant therapy. Breast cancer: targets and therapy. 2012; 2012(4):139–154.
8. Quesson B, Bouzier AK, Thiaudiere E, Delalande C, Merle M, Canioni P. Magnetization transfer fast imaging of implanted glioma in the rat brain at 4. 7 T: interpretation using a binary spin-bath model. J Magn Reson Imaging. 1997; 7(6):1076–1083. [PubMed: 9400852]
9. Kumar V, Jagannathan NR, Kumar R, Thulkar S, Gupta SD, Hemal AK, Gupta NP. Evaluation of the role of magnetization transfer imaging in prostate: a preliminary study. Magn Reson Imaging. 2008; 26(5):644–649. [PubMed: 18436407]
10. Barker GJ, Schreiber WG, Gass A, Ranjeva JP, Campi A, van Waesberghe JH, Franconi JM, Watt HC, Tofts PS. A standardised method for measuring magnetisation transfer ratio on MR imagers from different manufacturers--the EuroMT sequence. MAGMA. 2005; 18(2):76–80. [PubMed: 15785944]
11. Tofts PS, Steens SC, Cercignani M, Admiraal-Behloul F, Hofman PA, van Osch MJ, Teeuwisse WM, Tozer DJ, van Waesberghe JH, Yeung R, Barker GJ, van Buchem MA. Sources of variation in multi-centre brain MTR histogram studies: body-coil transmission eliminates inter-centre differences. MAGMA. 2006; 19(4):209–222. [PubMed: 16957936]
12. Henkelman RM, Huang XM, Xiang QS, Stanisz GJ, Swanson SD, Bronskill MJ. Quantitative Interpretation of Magnetization-Transfer. Magn Reson Med. 1993; 29(6):759–766. [PubMed: 8350718]
13. Gochberg DF, Kennan RP, Gore JC. Quantitative studies of magnetization transfer by selective excitation and T-1 recovery. Magn Reson Med. 1997; 38(2):224–231. [PubMed: 9256101]
14. Sled JG, Pike GB. Quantitative interpretation of magnetization transfer in spoiled gradient echo MRI sequences. J Magn Reson. 2000; 145(1):24–36. [PubMed: 10873494]
15. Gochberg DF, Fong PM, Gore JC. A quantitative study of magnetization transfer in MAGIC gels. Phys Med Biol. 2003; 48(21):N277–N282. [PubMed: 14653567]

16. Edzes HT, Samulski ET. The measurement of cross-relaxation effects in the proton NMR spin-lattice relaxation of water in biological systems: Hydrated collagen and muscle. J Magn Reson. 1978; 31(2):207–229.

17. Gochberg DF, Gore JC. Quantitative imaging of magnetization transfer using an inversion recovery sequence. Magn Reson Med. 2003; 49(3):501–505. [PubMed: 12594753]

18. Gochberg DF, Gore JC. Quantitative magnetization transfer imaging via selective inversion recovery with short repetition times. Magn Reson Med. 2007; 57(2):437–441. [PubMed: 17260381]

19. Li K, Zu Z, Xu J, Janve VA, Gore JC, Does MD, Gochberg DF. Optimized inversion recovery sequences for quantitative T1 and magnetization transfer imaging. Magn Reson Med. 2010; 64(2): 491–500. [PubMed: 20665793]

20. Dortch RD, Li K, Gochberg DF, Welch EB, Dula AN, Tamhane AA, Gore JC, Smith SA. Quantitative magnetization transfer imaging in human brain at 3 T via selective inversion recovery. Magn Reson Med. 2011; 66(5):1346–1352. [PubMed: 21608030]

21. Dortch RD, Moore J, Li K, Jankiewicz M, Gochberg DF, Hirtle JA, Gore JC, Smith SA. Quantitative magnetization transfer imaging of human brain at 7 T. Neuroimage. 2013; 64:640–649. [PubMed: 22940589]

22. Li, K.; Dortch, RD.; Bryant, ND.; Buck, AKW.; Towse, TF.; Gochberg, DF.; Does, MD.; Damon, BM.; Park, JH. In Vivo Transverse Relaxation and Magnetization Transfer Imaging of Human Thigh Muscles at 3.0 Tesla. Salt Lake City 3508: 2013 Apr.

23. Yarnykh VL. Pulsed Z-spectroscopic imaging of cross-relaxation parameters in tissues for human MRI: theory and clinical applications. Magn Reson Med. 2002; 47(5):929–939. [PubMed: 11979572]

24. Tozer DJ, Rees JH, Benton CE, Waldman AD, Jager HR, Tofts PS. Quantitative magnetisation transfer imaging in glioma: preliminary results. NMR Biomed. 2011; 24(5):492–498. [PubMed: 20960580]

25. Underhill HR, Rostomily RC, Mikheev AM, Yuan C, Yarnykh VL. Fast bound pool fraction imaging of the in vivo rat brain: association with myelin content and validation in the C6 glioma model. Neuroimage. 2011; 54(3):2052–2065. [PubMed: 21029782]

26. van Zijl PC, Yadav NN. Chemical exchange saturation transfer (CEST): what is in a name and what isn't? Magn Reson Med. 2011; 65(4):927–948. [PubMed: 21337419]

27. Colvin DC, Yankeelov TE, Does MD, Yue Z, Quarles C, Gore JC. New insights into tumor microstructure using temporal diffusion spectroscopy. Cancer Res. 2008; 68(14):5941–5947. [PubMed: 18632649]

28. Hu X, Le TH. Artifact reduction in EPI with phase-encoded reference scan. Magn Reson Med. 1996; 36(1):166–171. [PubMed: 8795036]

29. Maes F, Collignon A, Vandermeulen D, Marchal G, Suetens P. Multimodality image registration by maximization of mutual information. IEEE Trans Med Imaging. 1997; 16(2):187–198. [PubMed: 9101328]

30. Henkelman RM, Huang X, Xiang QS, Stanisz GJ, Swanson SD, Bronskill MJ. Quantitative interpretation of magnetization transfer. Magn Reson Med. 1993; 29(6):759–766. [PubMed: 8350718]

31. Rajan SS, Rosa L, Francisco J, Muraki A, Carvlin M, Tuturea E. MRI characterization of 9L-glioma in rat brain at 4. 7 Tesla. Magn Reson Imaging. 1990; 8(2):185–190. [PubMed: 2338899]

32. Cramer W. On the biochemical mechanism of growth. J Physiol. 1916; 50(5):322–334. [PubMed: 16993346]

33. Saryan LA, Hollis DP, Economou JS, Eggleston JC. Nuclear magnetic resonance studies of cancer. IV. Correlation of water content with tissue relaxation times. J Natl Cancer Inst. 1974; 52(2):599–602. [PubMed: 4406036]

34. Zhou J, Lal B, Wilson DA, Laterra J, van Zijl PC. Amide proton transfer (APT) contrast for imaging of brain tumors. Magn Reson Med. 2003; 50(6):1120–1126. [PubMed: 14648559]

35. Zhong JH, Gore JC, Armitage IM. Relative contributions of chemical exchange and other relaxation mechanisms in protein solutions and tissues. Magn Reson Med. 1989; 11(3):295–308. [PubMed: 2550719]

36. Wang S, Tryggestad E, Zhou T, Armour M, Wen Z, Fu DX, Ford E, van Zijl PC, Zhou J. Assessment of MRI parameters as imaging biomarkers for radiation necrosis in the rat brain. International Journal of Radiation Oncology Biology Physics. 2012; 83(3):e431–436.

37. Xu J, Zu Z, Zaiss M, Xie J, Gochberg DF, Bachert P, Gore JC. On the origins of chemical exchange saturation transfer (CEST) contrast in tumors at 9.4T. NMR Biomed. in press.

38. Xu J, Li K, Smith RA, Waterton JC, Zhao P, Chen H, Does MD, Manning HC, Gore JC. Characterizing tumor response to chemotherapy at various length scales using temporal diffusion spectroscopy. PLoS ONE. 2012; 7(7):e41714. [PubMed: 22911846]

39. Bailey C, Desmond KL, Czarnota GJ, Stanisz GJ. Quantitative magnetization transfer studies of apoptotic cell death. Magn Reson Med. 2011; 66(1):264–269. [PubMed: 21695728]

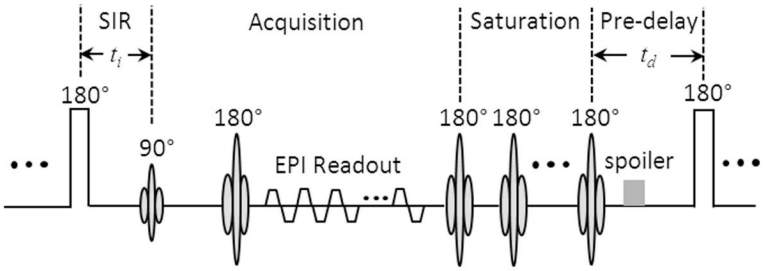

Figure 1.
Diagram of SIR-EPI sequence with a saturation pulse train applied after the EPI readout to saturate the free and macromolecular pools.

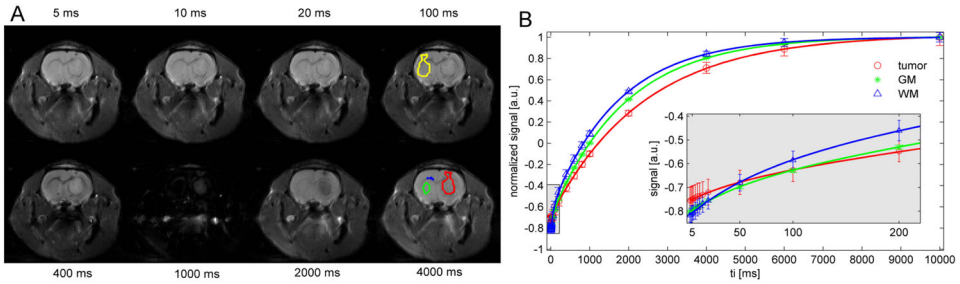

Figure 2.

(A) Representative eight SIR EPI images from total 20 images with different inversion times. The region-of-interest (ROI) boundaries of subcortical gray matter (green), corpus callosum white matter (blue), tumor (red) and contralateral normal tissue (yellow) are overlaid on the images. (B) The corresponding model fits of SIR signals normalized by corresponding signals at t_i = 10 sec. A magnified image with a logarithmic axis of inversion time is inserted to show the excellent agreement between the SIR-qMT data (open markers) and the bi-exponential model of Eq.[1] (solid lines) at short inversion times. The errorbars represent the standard deviations of ROI.

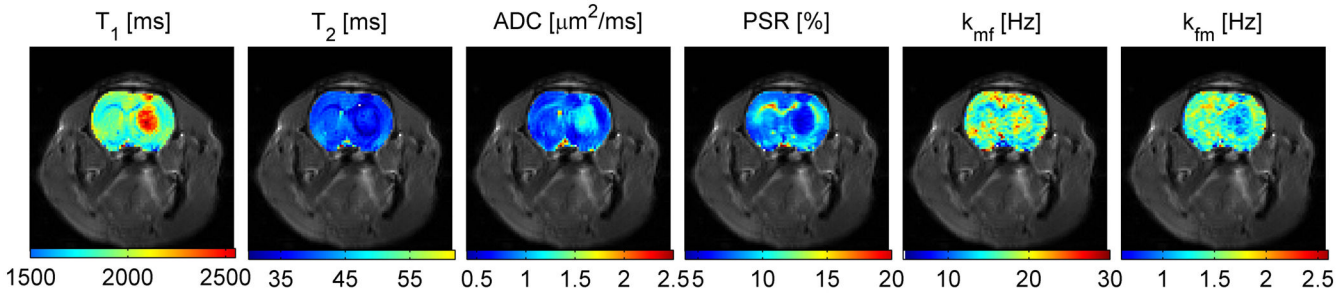

Figure 3.

Representative multiple parametric maps overlaid on a corresponding spin-echo EPI image. Note that PSR provides excellent differentiation of tumor, gray matter and while mater tissues. Although there is a clear contrast between gray matter and white matter, the overall k_{mf} and k_{fm} maps are much noisier.

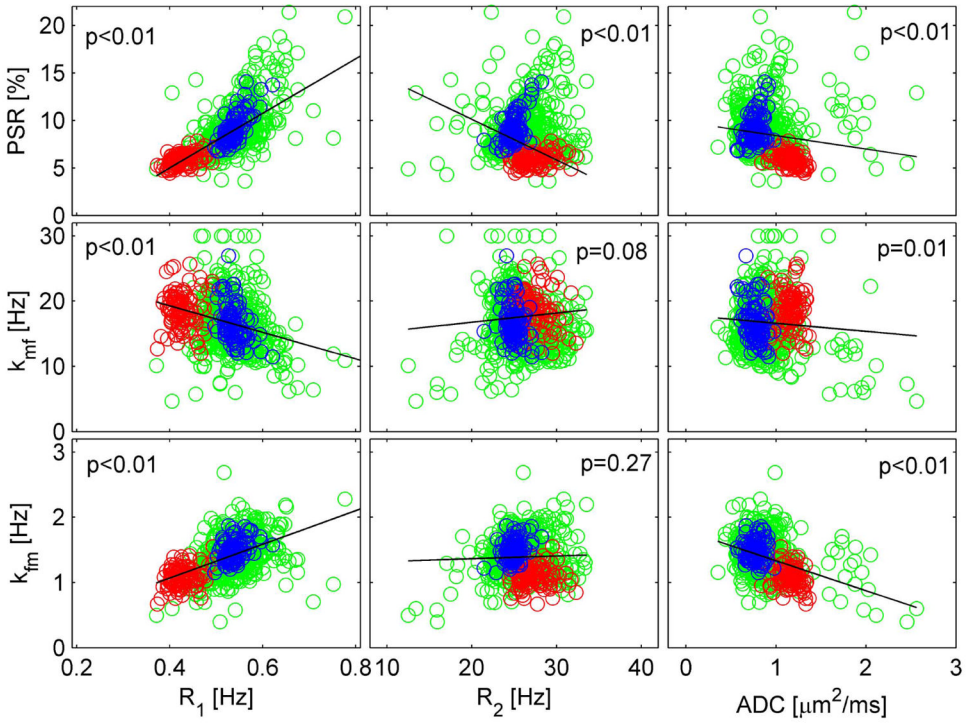

Figure 4.

Pixel-wise correlations between SIR-qMT parameters (PSR, k_{mf} and k_{fm}) and conventional MRI parameters (R_1, R_2 and ADC). Red circles represent pixels inside the tumor, blue for those in the contralateral normal tissue and green for all elsewhere brain tissue. The p value of the Pearson's correlation of all pixels in each subfigure was provided, and a corresponding linear regression fit was shown as black solid lines.

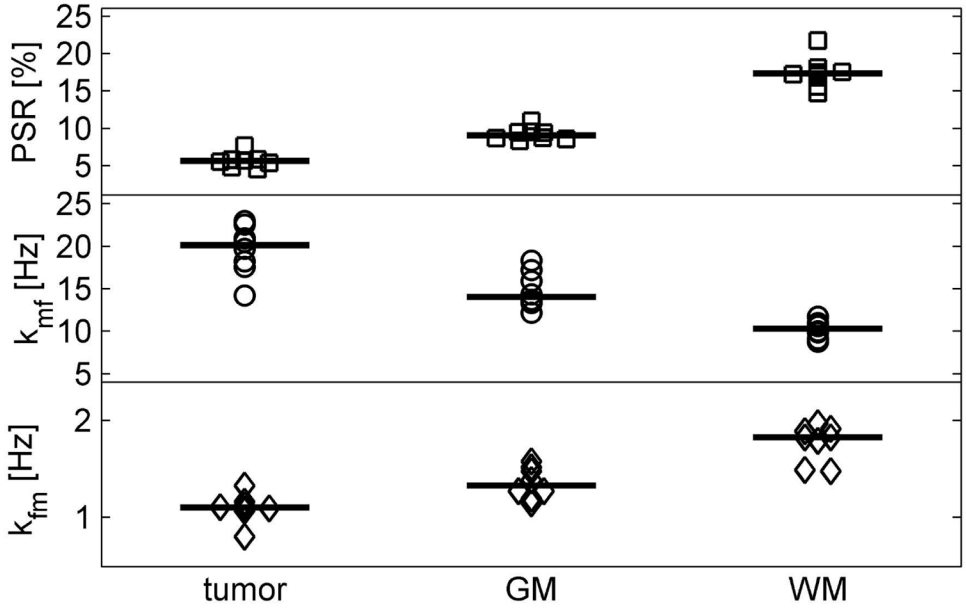

Figure 5.
Summary of fitted PSR (pool size ratio), k_{mf} and k_{fm} (MT exchange rate) of all eight animals. All parameters can differentiate different types of tissues, i.e. tumor, GM (gray matter) or WM (white matter) with statistical significance ($p<10^{-12}$, $p<10^{-7}$, and $p<10^{-8}$, respectively, given by balanced one-way ANOVA analyses).

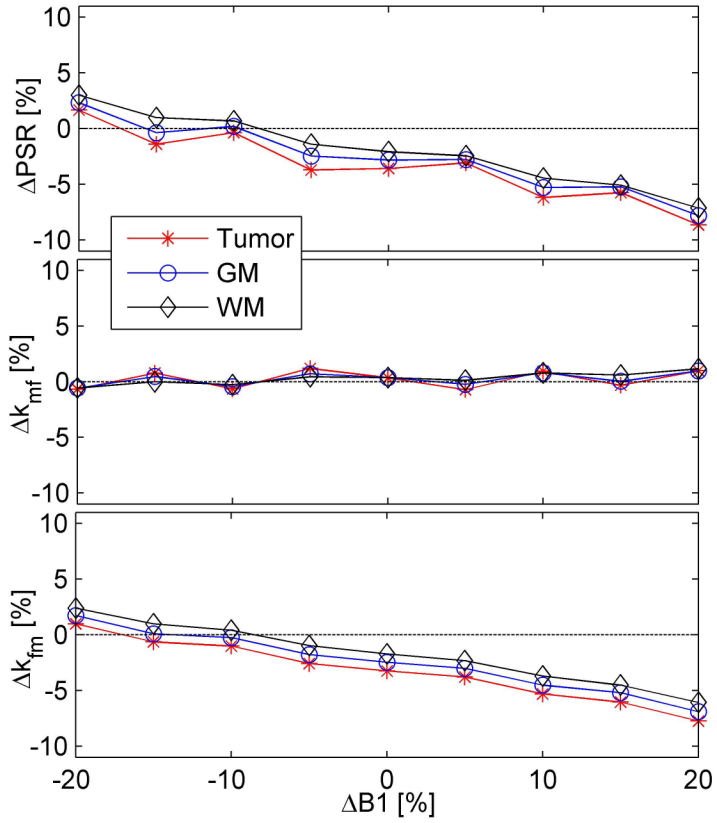

Figure 6.
Simulated relative errors of qMT parameters with the presence of saturation echo train, B_1 inhomogeneity and different relaxation times. Note that $k_{fm} = k_{mf} \times$ PSR.

Table 1

Summary of ROI-based parameter means ± standard deviations of all animals.

	R_1 [Hz]	R_2 [Hz]	ADC [$\mu m^2/ms$]	PSR [%]	k_{mf} [Hz]	k_{fm} [Hz]
Tumor	0.47±0.07	27.42±2.22	0.80±0.10	5.67±0.95	19.69±2.88	1.10±0.15
GM	0.59±0.05	24.91±0.26	0.68±0.03	9.20±0.86	14.82±2.12	1.35±0.16
WM	0.63±0.03	29.33±2.08	0.79±0.13	17.42±2.05	10.23±0.99	1.77±0.19

Table 2

Bonferroni-corrected p values for all pairwise comparisons in Figure 5.

	Tumor vs GM	Tumor vs WM	GM vs WM
PSR	1.83×10^{-6}	5.25×10^{-8}	1.22×10^{-6}
k_{mf}	0.012	3.91×10^{-5}	4.80×10^{-4}
k_{fm}	0.008	5.79×10^{-5}	3.45×10^{-4}